Efros-Shklovskii variable range hopping and nonlinear transport in 1T/1T′-MoS2

Papadopoulos, N.; Steele, G. A.; Van Der Zant, H. S.J.

Important note
To cite this publication, please use the final published version (if applicable).
Please check the document version above.

Efros-Shklovskii variable range hopping and nonlinear transport in $1T/1T'$-MoS$_2$

N. Papadopoulos,[*] G. A. Steele, and H. S. J. van der Zant

Kavli Institute of Nanoscience, Delft University of Technology, Lorentzweg 1, Delft 2628 CJ, The Netherlands

We have studied temperature- and electric-field-dependent carrier transport in single flakes of MoS$_2$ treated with n-butyllithium. The temperature dependence of the four-terminal resistance follows the Efros-Shklovskii variable range hopping conduction mechanism. From measurements in the Ohmic and non-Ohmic regime, we estimate the localization length and the average hopping length of the carriers, as well as the effective dielectric constant. Furthermore, a comparison between two- and four-probe measurements yields a contact resistance that increases significantly with decreasing temperature.

I. INTRODUCTION

Transition-metal dichalcogenides (TMDCs) form a family of van der Waals crystals with the general formula MX_2, where M is a transition metal and X a chalcogen atom. Molybdenum disulfide is the most known among the TMDCs and in its natural form ($2H$ phase) it is a layered semiconductor with a band gap of 1.3 eV in bulk and 1.8 eV in monolayers [1]. $2H$-MoS$_2$ has attracted a lot of interest due to its use in field-effect transistors (FETs) [2], photodetectors [3], and its rich spin-valley physics [4]. Unlike $2H$-MoS$_2$, the $1T$-MoS$_2$ phase has metallic properties and an octahedral structure [5]. This phase is metastable and relaxes to the distorted $1T'$ one with clustering of the Mo sites and the formation of Mo chains [6,7]. The $1T'$ phase is semiconducting whose band gap has not been measured directly, but calculations yield values ranging from 0.08 eV [8] to 0.8 eV [9].

High doping levels can cause a phase transition from the $2H$ to the $1T$ and $1T'$ phases, which can be achieved chemically via charge transfer through intercalation of alkali metals [10], by exposure to electron beam irradiation [11] or by metallic adatom adsorption on the surface [12]. This phase transition has been studied extensively and was found to take place with gliding of the sulfur atom planes [13]. Unfortunately, the above processes convert the $2H$ phase to the $1T$ and $1T'$ phases ($1T/1T'$), but they also leave some domains of the semiconducting $2H$ phase inside the MoS$_2$ lattice [14]. Nonetheless, the resulting sheets have very different electronic and chemical properties than the natural $2H$-MoS$_2$.

Although there is a large variety of studies on $1T/1T'$-MoS$_2$ and related heterostructures, there are not many investigations on their electrical properties. Recently, temperature-dependent two-terminal transport measurements showed that electrons in $1T/1T'$-MoS$_2$ from chemical treatment are localized inside the metallic patches of the $1T$ phase, leading to Mott variable range hopping (VRH) [15]. Here, we report on four- and two-probe measurements on few-layer $1T/1T'$-MoS$_2$ flakes, obtained from an n-butyllithium treatment. We find that the channel resistance increases dramatically as the temperature decreases. A comparison between the two measurement configurations yields a small contact resistance at room temperature that increases considerably at low temperatures. We

find that the temperature dependence of the resistance obtained with four-terminal measurements in the Ohmic regime fits the Efros-Shklovskii VRH mechanism better than the Mott-VRH model. Furthermore, we study the nonlinear transport at low temperatures with two-probe measurements. While at low bias (Ohmic regime) the temperature dependence of the resistance is strong, at high electric fields this dependence is suppressed and the device operates in the non-Ohmic and electric-field-activated regime [16].

II. RESULTS

A. Phase transition and fabrication

Thin MoS$_2$ flakes were obtained using the Scotch tape technique and transferred on 285 nm SiO$_2$/Si substrates via a poly(dimethylsiloxane) (PDMS) dry transfer method [17]. A transferred flake before the chemical treatment is shown in Fig. 1(a). The flakes were immersed in n-butyllithium (1.6 M in hexane) for more than 48 h, and after extraction, the substrates were washed with hexane and de-ionized water to remove excess lithium. After the chemical treatment, there is a color change of the flake, as can be seen in Fig. 1(b). Another way to verify the phase transition is with Raman spectroscopy. Figure 1(d) depicts the spectrum of a flake after extraction from the n-butyllithium solution (black line). The J_1, J_2, and J_3 peaks that originate from the $1T'$ phase (green labels), the A_{1g} peak from the $1T$ phase, as well as the E_g, E_{2g}^1, and A_{1g} peaks from remnant patches of the initial $2H$ phase can be seen [6,9]. The Raman spectrum therefore indicates that the phase transition was incomplete, in line with previous reports [14,18].

After inducing the phase transformation, we proceed to device fabrication, for which standard e-beam lithography was used with a single-layer poly(methyl methacrylate) (PMMA) resist. To preserve the $1T/1T'$ phases, heating the PMMA above 95 °C must be avoided, which is the temperature at which the $1T/1T'$ to $2H$ phase transition is expected to take place [5]. We have found that baking the PMMA resists at 87 °C in a vacuum oven for a couple of minutes is sufficient to preserve the $1T/1T'$ phase. This can be seen in Fig. 1(d), where the Raman spectrum before (black curve) and after baking (blue curve) is similar, indicating that there is no substantial composition change of the flake. In contrast, flakes with PMMA baked at 175 °C for 3 min show a significant
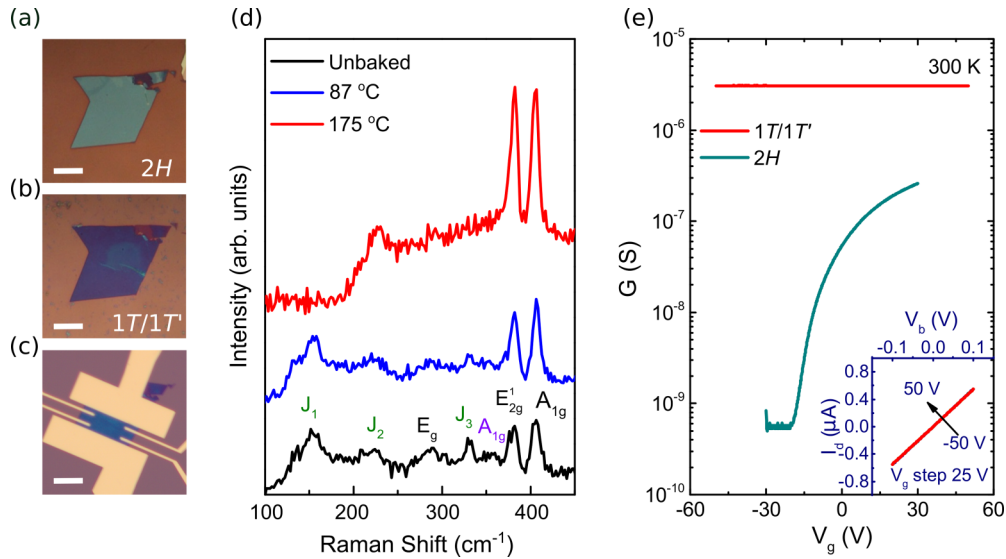
————

[*]n.papadopoulos@tudelft.nl

FIG. 1. Room-temperature characterization of $1T/1T'$-MoS$_2$ flakes and devices. Optical images (a) of an MoS$_2$ flake after exfoliation, (b) after immersion in n-butyllithium, and (c) of a fabricated device. Scale bar is 15 μm. (d) Raman spectra from $1T/1T'$-MoS$_2$ devices prepared under different conditions: unbaked (black line), baked at 87 °C (blue line), and baked at 175 °C (red line). (e) Two-terminal conductance as a function of the back-gate voltage for $2H$-MoS$_2$ (gray curve) and $1T/1T'$-MoS$_2$ (red curve). The inset shows the transfer characteristics of the $1T/1T'$ channel, for five back-gate voltages from -50 to 50 V with a step of 25 V; all curves fall on top of each other.

reduction in the intensities of the J_1, J_2, and J_3 peaks with a change in the background and an increase in the peak intensity from the $2H$ phase.

After PMMA patterning via e-beam lithography, e-beam metal evaporation was used to evaporate 5 nm of Ti and 70 nm of Au to form the contacts. Several Hall bars and other multiterminal devices for transport measurements have been fabricated. The advantage of n-butyllithium treatment and postfabrication, compared to a treatment after device fabrication, is that below the contacts there is $1T/1T'$-MoS$_2$, which can provide better Ohmic contacts according to earlier reports [19,20]. One of the final devices is shown in Fig. 1(c).

Figure 1(e) shows a room-temperature, two-probe electrical characterization of devices with $2H$ (gray) and $1T/1T'$-MoS$_2$ (red) flakes. The G-V_g curves were obtained by applying a dc voltage bias between the source and drain and measuring the source-drain current while sweeping the back-gate voltage. In the case of the sample with the $1T/1T'$-MoS$_2$, the back-gate modulation of the conductance is negligible, while in the untreated $2H$-MoS$_2$ sample the curve is semiconducting n type with a high on/off ratio. The zero transconductance in the case of the treated sample shows that the Fermi level lies inside the conduction band and that the material has a high electron density. The inset shows current-voltage characteristics from the device with the $1T/1T'$-MoS$_2$ channel at different back-gate voltages; these are linear, indicating Ohmic behavior.

B. Temperature dependence in the Ohmic regime

To investigate the electrical properties of thin $1T/1T'$-MoS$_2$ flakes, we studied their four- and two-terminal resistance as a function of temperature in two devices. Figure 2(a) shows current-voltage curves of two-terminal measurements that remain linear (Ohmic) down to liquid nitrogen temperatures.

The decreasing slope indicates that the resistance increases upon cooling. Using a four-probe configuration, we extract the resistance of the channel in the Ohmic regime as a function of temperature by applying currents of ±100 nA between the source and drain, while measuring the voltage drop across the channel. Figure 2(b) shows the two-probe and four-probe resistance as a function of temperature; both exhibit a strong temperature dependence displaying semiconductorlike behavior. The four-terminal resistance increases from 5 kΩ at room temperature to 180 kΩ at 90 K, while the two-probe resistance reaches 700 kΩ at 90 K. From these data, it is clear that although the $1T/1T'$ state shows a reduced resistance at room temperature and no gate voltage dependence, at low temperatures it exhibits an insulating state.

From the data in Fig. 2(b) the contact resistance of the device can be estimated from the formula $R_c = 0.5[R_{2T} - (l_{2T}/l_{4T})R_{4T}]$, where R_{2T} is the two-terminal and R_{4T} the four-terminal resistance, l_{4T} the length between the voltage probes, and where l_{2T} is the length between the current contacts. At 275 K, R_c is around 5.2 kΩ and increases considerably with decreasing temperature, reaching 70 kΩ at 90 K [Fig. 2(c)]. The contact resistance in the two devices was found to be less than 20% of the total resistance between 90 and 275 K.

To probe the nature of this localization, we analyze the temperature dependence of the four-terminal conductance of the device. The increase in the resistance indicates that the carrier transport takes place via hopping processes of the localized carriers. There are several models for hopping transport in solids. In the nearest-neighbor hopping model (NNH) the resistivity is proportional to $\exp(E_A/k_B T)$, with E_A the activation energy [21]. The general form for VRH-assisted transport on the other hand is $\rho \propto \exp[(T_0/T)^a]$, where T_0 is a characteristic temperature. For two dimensions and in the case of Mott-VRH, the exponent a is equal to $1/3$ and the electrons hop between states that are spatially further apart but
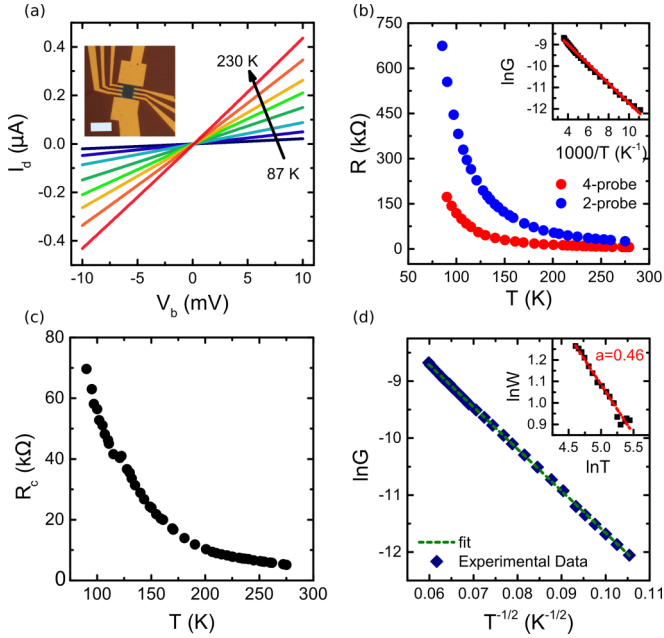
FIG. 2. Four-terminal transport measurements from room temperature to liquid nitrogen temperatures to determine transport mechanisms. (a) Current-voltage (I_d-V_b) characteristics from 87 to 230 K. In this temperature range, the observed low-bias I_d-V_b curves are linear with resistances below 1 MΩ. The inset shows an optical image of the device that was used. The scale bar is 7 μm. (b) Two-terminal (blue) and four-terminal (red) resistance as a function of temperature. The inset shows the dependence of natural logarithm of the four-terminal conductance from the inverse of the temperature $1000/T$. The deviation of the data from a linear relation (red line) indicates that the transport mechanism is not nearest-neighbor hopping. (c) Contact resistance as a function of temperature: At low temperatures, the contact resistance diverges. (d) $\ln G$ as a function of $T^{-1/2}$. The symbols are experimental data and the green dashed line the linear fit to them. The inset shows $\ln W$ (see main text for the definition) as a function of $\ln T$. The linear fit yields an exponent $a = 0.46 \pm 0.02$, consistent with the ES-VRH model.

closer energetically [22]. In the case of Efros-Shklovskii (ES) VRH, the exponent $a = 1/2$ and hopping takes place under the influence of strong electron-electron interactions [23].

As it can be seen from the inset of Fig. 2(b), which depicts the natural logarithm of the four-terminal conductance $\ln G$ as a function of $1000/T$, the data do not follow a straight line so that the NNH model cannot explain the conduction mechanism of $1T/1T'$-MoS$_2$. To analyze this further, one can plot $\ln G$ vs $T^{-1/2}$; in the case that the transport is governed by ES-VRH, the data should show a linear relation. The data in Fig. 2(d) show such a plot, and the linear relation indeed suggests an ES-VRH mechanism. To confirm the exponent, one can also plot $\ln W$ as a function of $\ln T$, where $W = -\partial \ln \rho / \partial \ln T \propto a(T_o/T)^a$. The slope of $\ln W$ vs $\ln T$ is equal to the exponent a. Such a plot is shown in the inset of Fig. 2(d). From a linear fit, we extract an exponent $a = 0.46 \pm 0.02$, close to the exponent expected for an ES-VRH mechanism [24,25]. Similarly, from a second device (device B), $a = 0.43 \pm 0.02$. Interestingly, if we do the same analysis for two-terminal measurements that include the contact resistance, we find

a slope for device A of 0.31 ± 0.02 and for device B of 0.49 ± 0.03, highlighting the importance of four-terminal measurements for the determination of such exponents.

Returning to the analysis of $\ln G$ vs T^{-a}, we can also compare different linear fits taken for different exponents for the temperature on the x axis. In the plot of $\ln G$ vs $T^{-1/2}$, a linear fit yields a residual sum of squares error of 0.0076. Similarly, in a plot of $\ln G$ vs $T^{-1/3}$ (not shown), the linear fit yields a value of the residual sum of squares error equal to 0.025. The smaller value of the residuals in the former case verifies that the Efros-Shkolvskii mechanism explains our results better than the Mott-VRH model. From this analysis, we can also extract the slope in a $\ln G$ vs $T^{-1/2}$ plot, from which the characteristic temperature of the ES hopping (T_{ES}) can be determined. For the two devices, we find a T_{ES} of 5426 K (device A) and 7898 K (device B).

C. Electric field dependence in the non-Ohmic regime

Another aspect of hopping conduction is the field-assisted motion of charge carriers between localized states [26]. This field-assisted hopping leads to nonlinear transport characteristics and above a critical electric field the conductivity becomes temperature independent. According to the ES-VRH model, the dependence of the resistivity from the electric field (E) is given by [16,27,28]

$$\rho \propto \exp(E_{ES}/E)^{1/2}, \tag{1}$$

where E_{ES} is a characteristic field connected to the localization length (ξ) and to T_{ES} by the relationship $E_{ES} = k_B T_{ES}/e\xi$ [27].

Below a critical field $E_c(T)$ transport follows an Ohmic dependence and is in the strongly temperature-dependent regime, since the phonons assist the hopping processes. Above $E_c(T)$ the carriers have enough energy to pass the Coulomb barrier and the temperature dependence is suppressed. As $E_c(T)$ is temperature dependent and decreases as temperature is lowered, nonlinear current-voltage curves are therefore more prominent at low temperatures; furthermore, at low temperatures, the channel resistance can become very high and four-terminal measurements are therefore more challenging for studying the electric field dependence of transport.

In Fig. 3(a) we plot two-terminal I_d-V_b curves of the device (device B in this case), at temperatures between 3.5 and 30 K; they are highly nonlinear. At a temperature of 3.5 K and with a bias of 4 V the resistance is 4.4 GΩ, while for 15 V it declines to 150 MΩ. Despite the high bias we did not observe an electrical breakdown of the devices. Note that the large channel and contact resistances (GΩ) do not allow one to perform four-terminal measurements due to the internal resistance of the voltmeter and the voltage limits of our isolation amplifiers. Nonlinear transport characteristics in the current-voltage curves in this device were also observed in four-terminal measurements at temperatures between 85 K and 105 K (see Fig. S1) [29], but the activationless regime is not accessible due to the high critical field (E_c) at these temperatures.

The crossover from strong to weak temperature dependence can be seen more clearly in Fig. 3(b), which depicts a semilogarithmic plot of the current as a function of temperature for different bias voltages (V_b). The plot indicates that the suppression of the temperature dependence takes place above 12 V.
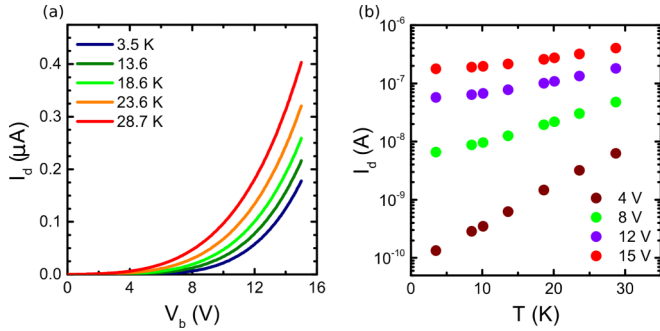
FIG. 3. Two-terminal nonlinear transport at low temperatures. (a) Nonlinear current-voltage characteristics at low temperatures. (b) Semilogarithmic plot of the current I_d as a function of temperature for different bias voltages V_b. The crossover from a strong temperature dependence to a weak temperature dependence of the channel current is more clearly seen.

This translates to an electric field of 2×10^6 V/m for a channel of 6 μm. At $V_b = 4$ V the ratio between the current at 3.5 and 30 K is on the order of 50, while for 15 V this ratio is about 2.

Assuming that the nonlinearity in the current-voltage curves arises from ES-VHR with a negligible contribution from the contacts, we can then extract the ES electric field from the non-Ohmic regime. The value of E_{ES} can be obtained by plotting the ln I_d as a function of $E^{-1/2}$, as depicted in Fig. 4 for different temperatures. As the electric field increases (left-hand side of the plot), the curves from different temperatures converge to a single line at the temperature-dependent critical field [$E_c(T)$]. Equation (1) indicates that a least-squares fit to the linear part of the ln I_d-$E^{-1/2}$ curve provides an estimate for E_{ES}. For the lowest temperature (3.5 K) which fulfills this condition, we obtain a slope of 14347 (V/m)$^{1/2}$ that corresponds to an electric field of 2.06×10^8 V/m (inset of Fig. 4). For the other device, E_{ES} is found to be 3.8×10^8 V/m.
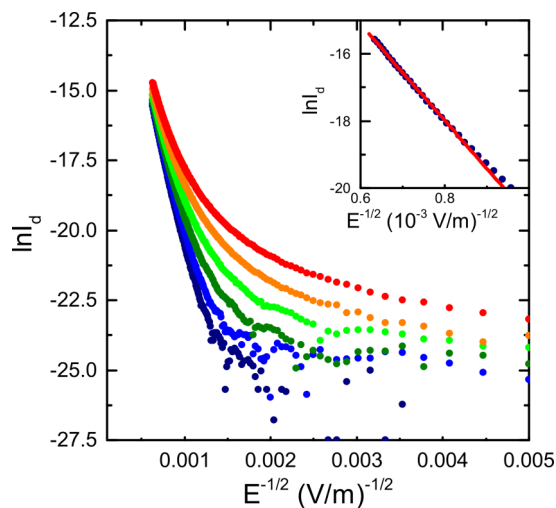

FIG. 4. Determination of the characteristic field E_{ES} from the nonlinear transport data. ln I_d as a function of $E^{-1/2}$ for temperatures of 3.5 K (navy), 8.6 K (blue), 13.6 K (dark green), 18.6 K (light green), 23.6 K (orange), and 28.7 K (red). The slope of the linear part at high electric fields and at 3.5 K yields the parameter $E_{ES}^{1/2}$ (inset).

III. DISCUSSION

From the values of E_{ES} and T_{ES} determined from the experiment, the localization length ξ can be estimated using the relationship $\xi = k_B T_{ES}/e E_{ES}$. For device A the localization length is 1.2 nm, while for device B the localization length is 3.3 nm. The average hopping length, which for ES-VRH is given by $\bar{r} = \xi(\frac{T_{ES}}{T})^{1/2}$ can be estimated using the experimental values of ξ and T_{ES}. At 300 K, the average hopping distances of the carriers in device A and device B are 5 and 17 nm, respectively. The obtained values of $\bar{r}$ favor the physical picture of electron hopping from one $1T$ phase patch to another, as previously suggested by Kim *et al.* [15].

Another parameter that can be calculated from the data is the effective dielectric constant of Li treated MoS$_2$, which in this case originates from the $1T'$ and $2H$ phases between the $1T$ phase domains. According to the ES-VRH model the critical temperature is given by [30]

$$T_{ES} = \frac{2.8e^2}{4\pi \epsilon_0 \epsilon_r k_B \xi}, \tag{2}$$

where e is the electron charge, ϵ_r is the dielectric constant, and ϵ_0 the electric permittivity of the vacuum. We estimate effective dielectric constants of 7 and 2 for the thick and thin flakes, in line with the order of magnitude expected for MoS$_2$ [31]. We note that this estimation of the dielectric constant does not take into account the possibly metallic character of the material, which could change the screening characteristics. To get better estimates of the effective dielectric constant in atomically thin materials, their two-dimensional (2D) nature should be taken into account [32].

We also note that in a previous work, Mott-VRH was observed in the transport behavior of n-butyllithium treated MoS$_2$ from two-terminal measurements, a hopping mechanism that is different compared to our analysis on data from four-terminal measurements [15]. We note, however, that an analysis of our two-terminal resistance data from device A can also be performed with the Mott-VRH model, with an exponent of $a = 0.31$ and a localization length of 0.7 nm, very similar to previous work [15], and in this sense the two data sets are not in contradiction.

Our observation of Efros-Shklovskii driven transport in $1T/1T'$-MoS$_2$ agrees with studies on similar systems [24,33,34]. Theoretical studies of irregular arrays of metallic grains, embedded in an insulating matrix resembling the n-butyllithium treated MoS$_2$ lattice, show that Coulomb interactions take place and that the transport follows the ES-VRH mechanism [33]. Similar results were obtained from electrical transport in two-dimensional graphene quantum dot arrays [34] and chemically reduced graphene oxide sheets [24].

Finally, the significant increase of the contact resistance in $1T/1T'$-MoS$_2$ suggests that the material is not the ideal candidate for contacting semiconducting $2H$-MoS$_2$ for experiments at cryogenic temperatures. Nevertheless, at room temperature, the measured R_c is low, which is in agreement with previous studies [19]. Measurements on devices with varying channel lengths (transfer length method) and studies on flakes with a higher content of the metallic $1T$ phase can provide more

insights regarding the behavior of the current injection into the $1T/1T'$ material.

IV. CONCLUSION

In summary, we observe Efros-Shklovskii-VRH transport in $1T/1T'$-MoS_2, as obtained from a treatment with n-butyllithium. From temperature-dependent measurements in the Ohmic regime and electric-field-dependent studies in the non-Ohmic and electric-field-driven regime, we obtain localization lengths in the order 1–3 nm. An interesting future direction of research could be to quantify and control the mixing of the different phases and observe how this affects the transport mechanisms.

[1] K. F. Mak, C. Lee, J. Hone, J. Shan, and T. F. Heinz, Phys. Rev. Lett. **105**, 136805 (2010).

[2] B. Radisavljevic, A. Radenovic, J. Brivio, V. Giacometti, and A. Kis, Nat. Nanotechnol. **6**, 147 (2011).

[3] O. Lopez-Sanchez, D. Lembke, M. Kayci, A. Radenovic, and A. Kis, Nat. Nanotechnol. **8**, 497 (2013).

[4] T. Cao, G. Wang, W. Han, H. Ye, C. Zhu, J. Shi, Q. Niu, P. Tan, E. Wang, B. Liu, and J. Feng, Nat. Commun. **3**, 887 (2012).

[5] F. Wypych and R. Schllhorn, J. Chem. Soc., Chem. Commun. **0**, 1386 (1992).

[6] S. J. Sandoval, D. Yang, R. F. Frindt, and J. C. Irwin, Phys. Rev. B **44**, 3955 (1991).

[7] X. R. Qin, D. Yang, R. F. Frindt, and J. C. Irwin, Phys. Rev. B **44**, 3490 (1991).

[8] X. Qian, J. Liu, L. Fu, and J. Li, Science **346**, 1344 (2014).

[9] T. Hu, R. Li, and J. Dong, J. Chem. Phys. **139**, 174702 (2013).

[10] N. Imanishi, M. Toyoda, Y. Takeda, and O. Yamamoto, Solid State Ionics **58**, 333 (1992).

[11] Y. Katagiri, T. Nakamura, A. Ishii, C. Ohata, M. Hasegawa, S. Katsumoto, T. Cusati, A. Fortunelli, G. Iannaccone, G. Fiori, S. Roche, and J. Haruyama, Nano Lett. **16**, 3788 (2016).

[12] A. N. Enyashin, L. Yadgarov, L. Houben, I. Popov, M. Weidenbach, R. Tenne, M. Bar-Sadan, and G. Seifert, J. Phys. Chem. C **115**, 24586 (2011).

[13] Y.-C. Lin, D. O. Dumcenco, Y.-S. Huang, and K. Suenaga, Nat. Nanotechnol. **9**, 391 (2014).

[14] G. Eda, T. Fujita, H. Yamaguchi, D. Voiry, M. Chen, and M. Chhowalla, ACS Nano **6**, 7311 (2012).

[15] J. S. Kim, J. Kim, J. Zhao, S. Kim, J. H. Lee, Y. Jin, H. Choi, B. H. Moon, J. J. Bae, Y. H. Lee, and S. C. Lim, ACS Nano **10**, 7500 (2016).

[16] F. Tremblay, M. Pepper, R. Newbury, D. Ritchie, D. C. Peacock, J. E. F. Frost, G. A. C. Jones, and G. Hill, Phys. Rev. B **40**, 3387 (1989).

[17] A. Castellanos-Gomez, M. Buscema, R. Molenaar, V. Singh, L. Janssen, H. S. J. van der Zant, and G. A. Steele, 2D Mater. **1**, 011002 (2014).

[18] D. Voiry, M. Salehi, R. Silva, T. Fujita, M. Chen, T. Asefa, V. B. Shenoy, G. Eda, and M. Chhowalla, Nano Lett. **13**, 6222 (2013).

[19] R. Kappera, D. Voiry, S. E. Yalcin, B. Branch, G. Gupta, A. D. Mohite, and M. Chhowalla, Nat. Mater. **13**, 1128 (2014).

[20] R. Kappera, D. Voiry, S. E. Yalcin, W. Jen, M. Acerce, S. Torrel, B. Branch, S. Lei, W. Chen, S. Najmaei, J. Lou, P. M. Ajayan, G. Gupta, A. D. Mohite, and M. Chhowalla, APL Mater. **2**, 092516 (2014).

[21] V. F. Gantmakher, *Electrons and Disorder in Solids*, No. 130 (Oxford University Press, Oxford, UK, 2005).

[22] N. F. Mott, Philos. Mag. **19**, 835 (1969).

[23] A. L. Efros and B. I. Shklovskii, J. Phys. C **8**, L49 (1975).

[24] D. Joung and S. I. Khondaker, Phys. Rev. B **86**, 235423 (2012).

[25] C.-I. Liu, B.-Y. Wu, C. Chuang, Y.-C. Lee, Y.-J. Ho, Y. Yang, R. E. Elmquist, S.-T. Lo, and C.-T. Liang, Semicond. Sci. Technol. **31**, 105008 (2016).

[26] B. Shklovskii, Sov. Phys. Semicond. **6**, 1964 (1973).

[27] A. V. Dvurechenskii, V. A. Dravin, and A. I. Yakimiv, JETP Lett. **48**, 155 (1988).

[28] D. Yu, C. Wang, B. L. Wehrenberg, and P. Guyot-Sionnest, Phys. Rev. Lett. **92**, 216802 (2004).

[29] See Supplemental Material at http://link.aps.org/supplemental/10.1103/PhysRevB.96.235436 for current-voltage characteristics from four-terminal measurements at low temperatures.

[30] B. I. Shklovskii and A. L. Efros, *Electronic Properties of Doped Semiconductors* (Springer, Berlin, 1984).

[31] S.-L. Li, K. Tsukagoshi, E. Orgiu, and P. Samor, Chem. Soc. Rev. **45**, 118 (2016).

[32] L. V. Keldysh, JETP Lett. **29**, 658 (1979).

[33] I. S. Beloborodov, A. V. Lopatin, and V. M. Vinokur, Phys. Rev. B **72**, 125121 (2005).

[34] D. Joung, L. Zhai, and S. I. Khondaker, Phys. Rev. B **83**, 115323 (2011).